Journal of Hydrology 601 (2021) 126491

Contents lists available at ScienceDirect

Journal of Hydrology

journal homepage: www.elsevier.com/locate/jhydrol

Research papers

Up and down: Bidirectional fluxes of fog droplets at two subtropical mountain forest sites

Bettina Breuer [a,*,1], Otto Klemm [a], Yen-Jen Lai [b], Po-Hsiung Lin [c], Heta Meyer [a,d], Felix Nieberding [a,e], Qing-Hai Song [f]

[a] Climatology Research Group, University of Münster, Heisenbergstr. 2, 48149 Münster, Germany
[b] Experimental Forest, National Taiwan University, Chien-Shan Road 12, Nantou, Taiwan, ROC
[c] Department of Atmospheric Sciences, National Taiwan University, 10617 Taipei, Taiwan, ROC
[d] Vegetation Ecology, Hochschule Weihenstephan-Triesdorf, Am Hofgarten 1, 85354 Freising, Germany
[e] Institute of Geosystems and Bioindication, Technische Universität Braunschweig, Langer Kamp 19c, 38106 Braunschweig, Germany
[f] Key Lab of Tropical Forest Ecology, Xishuangbanna Tropical Botanical Garden, Chinese Academy of Sciences, Menglun, Yunnan 666303, China

ARTICLE INFO

Keywords:
Fog droplet fluxes
East Asia
Eddy covariance
Bidirectional fluxes

ABSTRACT

Bidirectional fog droplet fluxes were observed at two mountainous subtropical forests in East Asia. To investigate the various boundary conditions and that cause these bidirectional droplet fluxes, we set up identical eddy covariance systems including a droplet spectrometer (FM100 Fog monitor) at two study sites in the Ailaoshan (SW China) and Xitou (central Taiwan) areas for several weeks in winter 2015/2016 and spring 2017, respectively. Normally, fog droplets are expected to have a downward flux toward the surface for all sizes due to impaction at the vegetation's surface. However, we also observed temporally positive fluxes, for fog droplets up to a diameter of 10 µm. Two different cases of bidirectional fog droplet fluxes were identified in our experiments: At Xitou, the positive droplet number fluxes for smaller droplets occurred together with a positive sensible heat flux in combination with large critical diameters according to the Köhler theory. At Ailaoshan, similar fluxes occurred yet together with negative sensible heat fluxes in combination with small critical diameters. We analyze the occurrence of these bidirectional droplet number fluxes in conjunction with the boundary layer conditions and the activation state of the droplets with diameters up to 10 µm. Plausible reasons for the identical flux directions at the two sites under very different microphysical fog conditions are presented.

1. Introduction

In the atmosphere, fog forms when the air is supersaturated with respect to water: The condensation of water vapor on hygroscopic aerosol particles, reduces the visibility and, thus, leads to the formation of fog (Pruppacher and Klett, 1996), which reduces visibility and, thus, leads to the formation of fog near the earth's surface. It is both the number concentration of fog droplets and their size distribution that determine the amount that visibility is reduced (Gultepe et al., 2007).

Fog droplets and aerosol particles greatly affect human life and nature (Hewson, 1943; Mildenberger et al., 2009). For example, fog plays an important role in ecosystem functioning through its participation in hydrological and biogeochemical cycles. Fog is a complex and dynamic phenomenon, that is often neglected. Fog research started long ago (Willett, 1928; Petterssen, 1939; Hewson, 1943; Best, 1951) and has focused on various aspects (visibility, liquid water content, hydrological input, modeling, remote sensing of fog etc.). Forests are fragile ecosystems and highly affected by climate change (Sperling et al., 2004; Zhou et al., 2013) and they interact with chemical and physical processes in fog (El-Madany et al., 2016; Burkard et al., 2003; Thalmann et al., 2002; Lovett, 1984; Eugster et al., 2006; Beiderwieden et al., 2008, 2007; Simon et al., 2016; Gultepe and Isaac, 2004). Our scope is to study the turbulent exchange processes of foggy air masses with the underlying forest ecosystem in order to further develop our basic understanding of these processes and their contribution to hydrological cycle.

Instruments for fast (10 Hz), size-resolved droplet measurements

* Corresponding author.
E-mail addresses: bettina.breuer@uni-muenster.de (B. Breuer), otto.klemm@uni-muenster.de (O. Klemm), alanlai@ntu.edu.tw (Y.-J. Lai), polin@ntu.edu.tw (P.-H. Lin), heta.meyer@hswt.de (H. Meyer), f.nieberding@tu-braunschweig.de (F. Nieberding), sqh@xtbg.ac.cn (Q.-H. Song).
[1] https://www.uni-muenster.de/Klima/team/BettinaBreuer.shtml

https://doi.org/10.1016/j.jhydrol.2021.126491
Received 8 January 2021; Received in revised form 20 May 2021; Accepted 22 May 2021
Available online 1 June 2021
0022-1694/

have been available for about 30 years. The first studies of turbulent fog droplet fluxes were conducted around 1990 (Beswick et al., 1991; Gallagher et al., 1988) and still, there are only a few research groups around the world studying this topic. The focus of most fog studies of turbulent fog droplet fluxes has been on water deposition due to turbulence to the ecosystem (Gallagher et al., 1992; Vong and Kowalski, 1995; Kowalski and Vong, 1999; Vermeulen et al., 1997; Thalmann et al., 2002; Eugster et al., 2006; Holwerda et al., 2006; Chang et al., 2006; Beiderwieden et al., 2008; Hiatt et al., 2012; Yamaguchi et al., 2015). However, studies have also found positive droplet fluxes for small droplets with diameters of up to 8 μm (Vong and Kowalski, 1995; Klemm and Wrzesinsky, 2007). Nonetheless, this change of flux direction within the size domain of droplets has not been a main research focus. Only one study by El-Madany et al. (2016) discussed possible causes of positive droplet fluxes. This study discussed the occurrence of bidirectional fluxes in mountainous terrain, but also in flat terrain positive flux have been found for droplet sizes up to 35 μm. (Vermeulen et al., 1997; Degefie et al., 2015a). In general, bidirectional fluxes do not lead to an overall positive (upward) flux of liquid water, because the liquid water content (LWC) in foggy air is dominated by the large droplets, which show negative (downward) fluxes. However, the common observation of positive fluxes of small droplets means that we need a better understanding of the processes that generally occur during the interaction of fog with the surface and within the fog layer.

As such, we take a closer look at all processes occurring in different areas of the fog layer and describe their effects on the droplets of different size classes. We merge different theories and observations of cloud physics and boundary layer processes to explain the origin of the positive fluxes. We also consider the fact that the processes by which fog droplets form and grow depend on the dissolved ion concentrations in the droplets and on the ambient vertical humidity gradient.

In our study, we focus on microphysical fog processes in mountainous terrain in subtropical forests, which are frequently exposed to foggy conditions. The goal of this study is to evaluate the processes driving bidirectional fog droplet fluxes in an environment. Thus, our research questions are: (I) What are sources and sinks of small droplets? (II) What causes bidirectional fluxes of fog droplets? (III) Does it depend on air pollution or other boundary layer conditions?

2. Materials and methods

2.1. Experimental setup and study sites

An eddy covariance (EC) system was set up at two sites in Southeast Asia, namely the flux tower at Ailaoshan National Natural Reserve in Yunnan Province, China (AS: 24.54219 N, 101.02959 E, 2476 m asl) and the Xitou flux tower in the Experimental Forest of National Taiwan University (XT: 23.66460 N, 120.79526 E, 1150 m asl) (see Fig. 1). An identical setup (full instrumentation see Table 1) was used at both sites: an EC system (10 Hz sample frequency) consisting of a droplet spectrometer FM100 and an R-50 sonic anemometer. The FM100 was orientated into the main wind direction under foggy conditions to avoid particle losses, as described by (Spiegel et al., 2012). Additionally, a PWD-11 was used to measure the visibility. Whenever the visibility dropped below 1000 m (10-min mean), an active fog collector (modified CALTECH design) was switched on (Degefie et al., 2015b). Fog water samples were usually taken every 0.5 h to 2 h, depending on the amount of water collected (Simon et al., 2016). Measurements of volume, pH and conductivity were performed as soon as possible after fog water collection. For detection of major ion concentrations the samples were analyzed with a ion chromatograph later on. Detailed methods of fog

Table 1
Overview of all used instruments.

	Instrument	Producer	Observed parameters
short-term	R-50 sonic anemometer	Gill Instruments, Ltd., Lymington, Hampshire, UK	wind speed wind direction u, v & w
	Fog monitor FM100	Droplet Measurement Technology, Boulder, Colorado, USA	droplet number concentration
	Present Weather Detector PWD-11	Vaisala Oyj, Helsinki, Finland	visibility
	Active fog collector (mod. CALTECH design)	in–house design, Germany	LWC
long-term	CSAT3 3-D sonic anemometer	Campell Scientific, Logan, Utah, USA	wind speed wind direction
	LI-7500 CO_2/H_2O infrared gas analyzer	LI-COR Bioscience, Lincoln, Nebraska, USA	CO_2 H_2O
	HMP45C	Vaisala Oyj, Helsinki, Finland	temperature RH

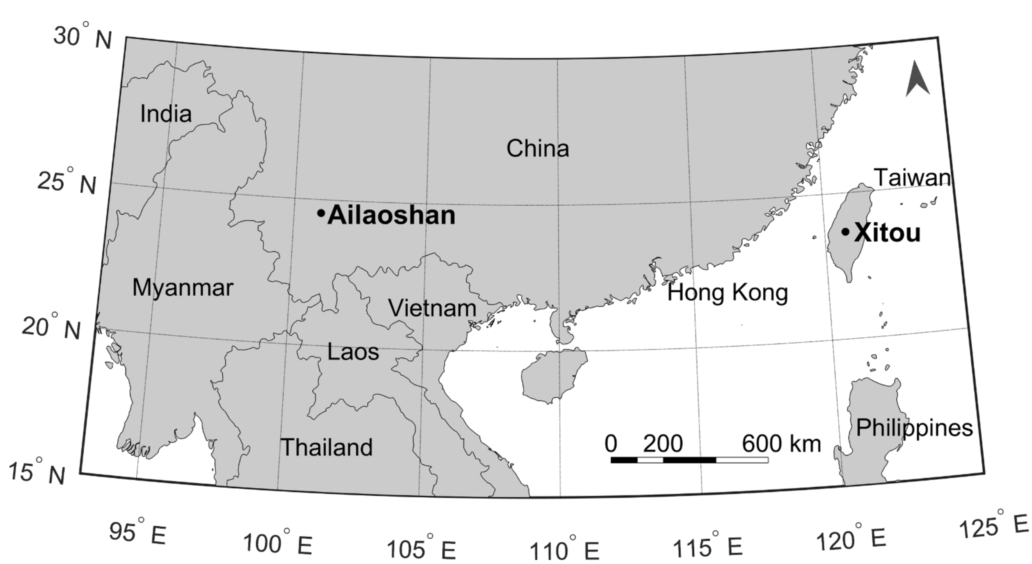

Fig. 1. Study sites at Ailaoshan (China) and Xitou (Taiwan).

water collection for AS was described by Nieberding (2017). The only difference for XT is, that the ion chromatographis analysis was conducted at the Department of Atmospheric Science of the National Taiwan University. In addition to this short-term investigation, permanent EC measurements are present at both sites, where instrumentation consists of an LI-7500 CO_2/H_2O infrared gas analyzer and a CSAT3 sonic anemometer (Table 1). Low frequency air temperature senors are mounted at each tower.

At the AS site, the measuring period was from January 2016 through March 2016. The flux tower is located on a northwest-oriented slope (around 15°) of a side valley in an old-grown evergreen broad-leaved forest (see Fig. 2 right panel). The flux system was installed at 31.6 m above ground level, which is about 6 m above the canopy. The main wind direction SW is caused by channeling of the valley (Nieberding et al., 2018). The average annual temperature at the study site is 11.3 °C and the annual average precipitation is 1840 mm (Tan et al., 2011). The monsoon climate produces a wet season from May to October and a dry season from November to April (Schaefer et al., 2009; Shi and Zhu, 2009). During the wet season (dry season), the average monthly precipitation varies from 100 mm to 500 mm (normally less than 50 mm) (Song et al., 2017). The driest month is March with almost no precipitation. Thus, the measurement period was within the dry season. Furthermore, fog events are frequent at the study site throughout the year with a peak during the wet season in summer. We presume mostly orographic lifting for the occurrence of fog, but there is no detailed analysis of the processes leading to foggy conditions (Nieberding et al., 2018).

At the XT site, the measuring period was in March 2017. The flux tower is located in a coniferous forest dominated by *Cryptomeria japonica* (Simon et al., 2016). The XT tower is situated in a relatively flat area within a valley with S to N orientation (slope of 15°) (see Fig. 2 left panel) (Simon et al., 2016). The occurrence of fog is strongly associated with wind directions from the north, and the fog is formed orographically as a result of adiabatic cooling during uphill transport from the valley. The flux system was installed at 40 m above ground level, which is 10 m above canopy height. The average temperature at the study site is 16.6 °C and the annual average precipitation is 2635 mm (Simon et al., 2016). There are two seasons at XT: a dry season from October to April and a wet season from May to September (Simon et al., 2016). Like at AS, the measuring period was during the dry season (March 2017). The fog frequency at XT is high with around 58% foggy days (min. 1 h d^{-1}), and the fog occurs usually during daytime based on our data. Fog events peak during the dry season.

2.2. Data pre-processing

For this study the definition of fog as described by WMO (2006) was used: In fog, the horizontal visibility is reduced to below 1000 m by the presence of hydrometeors. The definition was applied on the basis of 10-min averages of the PWD-11 signal. At AS, fog occurred for a total of 386 h of fog during the measuring period, which is equivalent to 34% of the total measurement period of 46 days. At XT, 177 h of fog were detected (25% of 29 days). Due to power shortages and freezing, 100 h (14%) of data were lost. At XT, we had only very few data losses (less than 2%).

Several steps of raw data pre-processing needed to be performed before calculating the droplet number fluxes and the liquid water fluxes (LWF). In general, the FM100 counts all droplets with a diameter between 2 µm and 50 µm and associates them with one of 40 channels in this range. The droplet detection operates on the principle of non-linear Mie scattering (Mie, 1908), in case of the FM100 at a wavelength of 680 nm. However, the non-linearity of Mie scattering causes some problems. For instance, a certain scattering intensity may corresponds to up to three different droplet sizes. Two methods are available to solve this issue: a stochastic approach by Spiegel et al. (2012) and a field-based approach by Gonser et al. (2011). For the present study, the field-based method was applied, i.e., the 40 measuring channels were merged into 23 size classes. Also, a smoothing filter (Savitzky and Golay, 1964) between the channels was applied to the data to reduce over- or underestimation of single size classes (Gonser et al., 2011). The FM100 raw data (counts per size class) were converted to number concentrations (droplets per cubic meter) with the optical sample area and the actual air flow. The actual air flow inside the instrument was measured with a pitot tube with a relatively constant air speed of 13.02 m s^{-1}. In cases where the pitot tube was blocked with fog water, the air flow could not be calculated correctly and the value became comparably small or high. Such erroneous air flows with deviations of more than ±1 m s^{-1} of the mean air speed were replaced with the mean value (13.02 m s^{-1}) (El-Madany et al., 2016; Wrzesinsky, 2003). For calculating the LWC and LWF, each size class was converted into a droplet diameter by using the geometric mean channel diameter with the assumption of spherical droplet shapes. The size classes are not distributed equidistantly and each class covers a different size range. Therefore, all number concentrations, liquid water contents and associated fluxes were normalized by their respective class widths (El-Madany et al., 2016). This makes data more comparable to each other.

2.3. Flux calculation

After pre-processing the data, we calculated the turbulent fluxes of

Fig. 2. Detailed satellite view of the study sites at Ailaoshan (right, China) and Xitou (left, Taiwan).

the FM100/R3-50 system with EddyUH (Mammarella et al., 2016).

The fluxes of the permanent measurements were calculated with EddyPro (LI-COR Biosciences).

For our short-term investigation with the FM100 data, we used the coordinate rotation method planar fit (Wilczak et al., 2001) because it is suitable for instrumentation set ups on a slope. With this method, the coordinate system is rotated according to the mean streamlines (Paw et al., 2000). Spikes in the raw data originating from random noise in the instruments (Brock, 1986) and from water deposition on the transducers of the sonic anemometer (Foken et al., 2004) were removed using the method of Vickers and Mahrt (Vickers and Mahrt, 1997). Regarding the flux calculation itself, we used the approach outlined in Horst (1997) for both scalar model cospectrum correction and for cospectral peak frequency vs. stability parameterization. The theoretical approaches by Moncrieff et al. (1997) and Rannik and Vesala (1999) were used to correct high and low frequency losses of sonic anemometer fluxes, respectively. Time lags were determined by maximizing the covariance within a predefined lag window of 2.5 s.

For our data, two different quality flags are available: the flux stationarity test (FST) and the integral turbulence characteristics (ITC) (Foken and Wichura, 1996). As our measurements were made at a slope, a temporarily positive momentum flux may occur; this leads to problems with interpreting the ITC for the vertical wind component. As the FST is not affected by the terrain, we used FST flagging only. We denoted all data with poor quality, (being flagged with values of 7 to 9) with gray pixels in the respective graphs (Figs. 4a&b, 5a&b). The data quality for most fog events was good; only some very small fluxes had to be discarded due to bad quality.

2.4. Kóhler theory

We used a theoretical approach to compare the ion concentrations in the droplets and their effects on droplets sizes. The Kóhler theory (Köhler, 1921; Seinfeld and Pandis, 2006) describes the equilibrium thermodynamics of droplets suspended in the gas phase with high relative humidity (RH). This theory describes the combination of the Kelvin effect and the Raoult Law. In general, deliquesced aerosol particles exist in a stable equilibrium at sizes below their critical diameters and at an RH of below 100% up to just over 100%, while their growth is accelerated once the critical diameter is exceeded. In this case, the aerosol particles are called activated cloud condensation nuclei (CCN), sometimes also called fog nuclei.

To calculate Kóhler curves and the respective critical diameters of the fog events at our study sites, we estimated the median ion concentration for single droplets. First, the particle mass (PM) of a single droplet was estimated as

$$PM = IC_{sum} \cdot \frac{LWC_{median}}{DNC_{median}}$$

where IC [g l^{-1}] is the liquid water ionic concentration of all measured species, LWC [l m^{-3}] is the liquid water content based on the data of the fog collector (Simon et al., 2016), and DNC [m^{-3}] is the droplet number concentration measured with the FM100. The Kóhler curve for each site was calculated with the particle mass PM [g] (Seinfeld and Pandis, 2006). An overview of all chemical components is shown in Table 2. The results were inserted to the following equation according to the Kóhler theory (Seinfeld and Pandis, 2006):

$$e = e^0 exp\left(\frac{A}{D_p} - \frac{B}{D_p^3}\right)$$

with the terms A and B:

$$A = \frac{4M_w\sigma_w}{RT\rho_w}$$

$$B = \frac{6n_sM_w}{\pi\rho_w}$$

where in detail e is the actual water vapor pressure over the droplet, e^0 is the water vapor pressure over a flat surface, σ is the air–water surface tension, M_w is the molecular weight of water, R is the molecular gas constant, T is the temperature, ρ is the water density, D is the droplet/particle diameter, and n_s is the number of solute moles. The critical diameter D_{pc} can be calculated with

$$D_{pc} = \left(\frac{3B}{A}\right)^{0.5}$$

Note that such estimates cannot be more than rough estimates, because the conditions change fast between events and even temporally and spatially within single fog events.

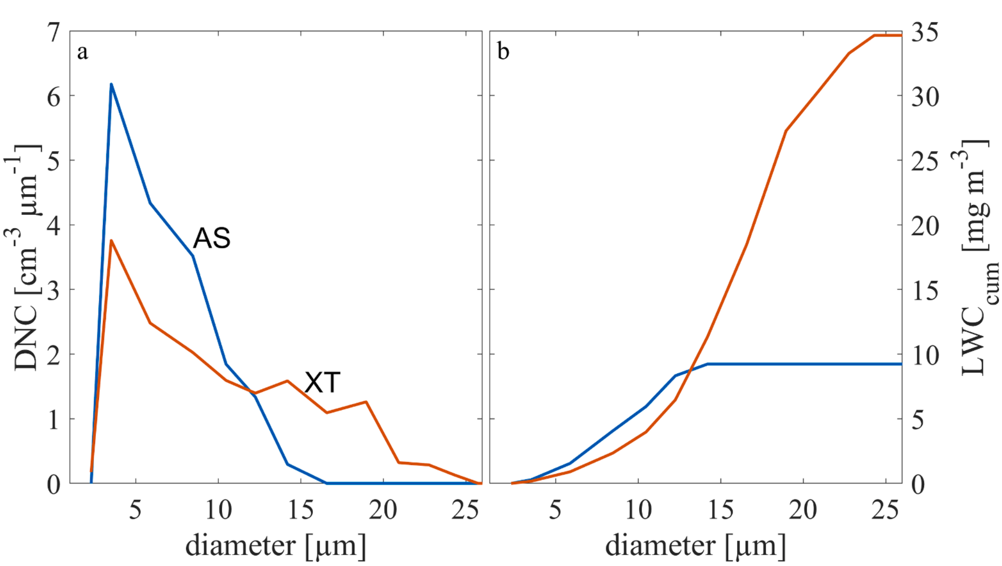

Fig. 3. Droplet Size Distributions of the two fog events, at AS (blue) and XT (orange). Only the dense center section of the fog event was selected to avoid edge effects (AS: 1st/2nd March 22:00 h to 8:00 h, XT: 9th March 12:00 h to 19:00 h). Panel a shows the droplet number concentrations (DNC) and panel b shows the cumulative liquid water content (LWC$_{cum}$), both as functions of droplet diameters.

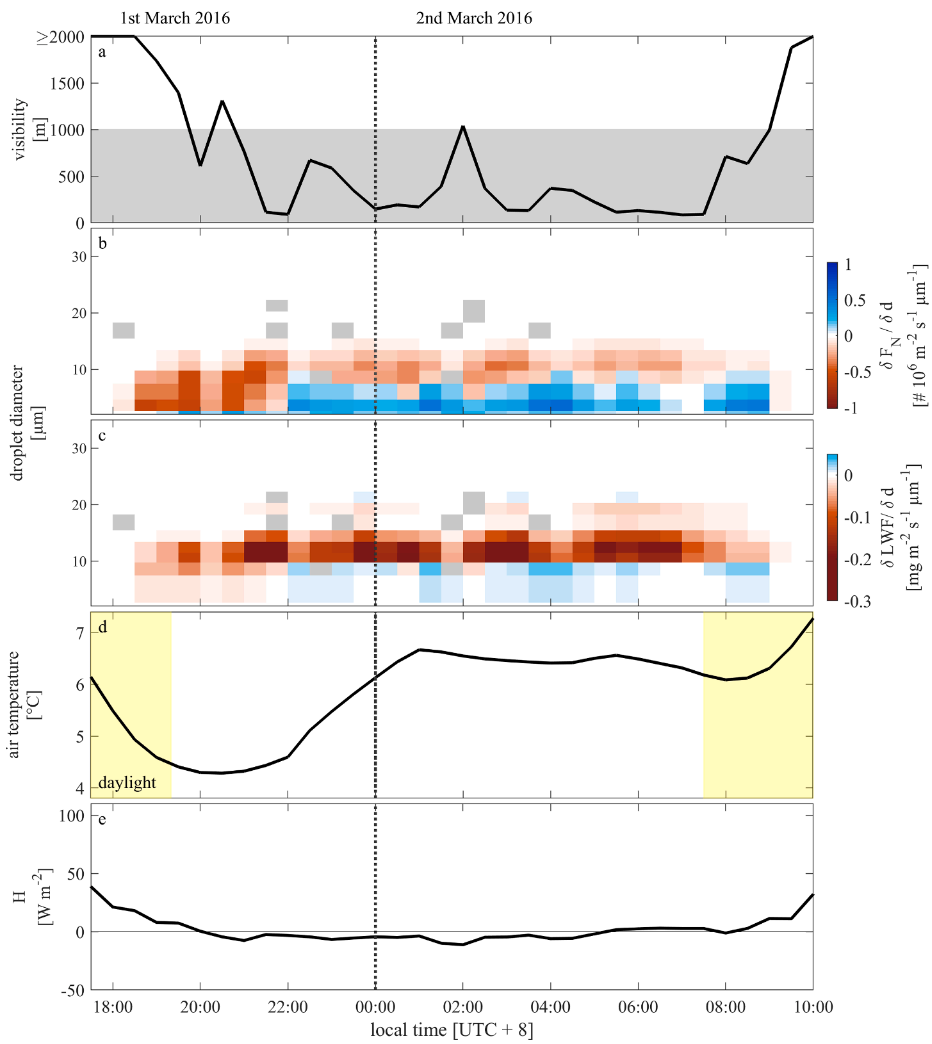

Fig. 4. Time series of the fog event on 1st and 2nd of March 2016 at AS showing the visibility (a), the normalized size-resolved droplet number flux (b), the normalized size-resolved LWF (c), the air temperature (d) and the sensible heat flux (e). The threshold of fog (visibility ⩽1000 m) is marked gray in panel a. Positive fluxes in panel b and c are shown in blue while negative fluxes are in red. Fluxes with bad quality flags (7, 8, 9) are denoted by gray pixels. White pixels are fluxes around zero, which also could be a result of low DNC.

Table 2
Fog event statistics for fog water at AS and XT. All ion concentrations in μeq l^{-1}. The dry particle mass of a single droplet was calculated with the droplet number concentration and the chemical composition.

	AS (median)	XT(median)
number of samples	3	11
pH	3.81	5.17
electric conductivity [μS cm^{-1}]	159	121
Ca^{2+}	67	27
Mg^{2+}	16.2	6.8
K^{+}	30	20
Na^{+}	11.7	12.7
H^{+}	154	6.8
NH_4^{+}	410	820
Cl^{-}	21	36
SO_4^{-}	450	240
NO_3^{-}	103	440
dry particle mass of a single droplet [mol]	9.1 x 10^{-16}	9.1 x 10^{-13}

3. Results

3.1. Meteorology

At both sites, the occurrence of fog was associated with a certain wind direction, SW at Ailaoshan and N at Xitou. Upslope winds cool adiabatically, the relative humidity increases and orographic clouds develop, which are recorded as fog at the meteorological research stations. The wind speed at AS was 2 ms^{-1} to 4 ms^{-1}, and at XT it was up to 3.5 ms^{-1}. The turbulence was well developed during fog events at AS (friction velocity $u_* \geqslant 0.3$ ms^{-1}). At XT, u_* was between 0.07 ms^{-1} and 0.3 ms^{-1} during foggy conditions. The average vertical wind speed before application of the planar fit rotation (see Section 2.3) at AS was positive all time between 0.04 ms^{-1} and 0.40 ms^{-1}, median 2.5 ms^{-1}. At XT, the pre-planar fit wind speed was between −0.24 ms^{-1} and +0.55 ms^{-1}, median +0.16 ms^{-1}. Negative values occurred only in the first and last hour of the fog event. At both sites, the latent heat flux was reduced to and subsequently fluctuated around zero W m^{-2} during the fog events.

3.2. Droplet size distribution

The droplet size concentration (DNC) and the liquid water content (LWC) are shown Fig. 3. At AS, the peak of the DNC was higher, but the diameters (see Fig. 3a), were smaller with virtually no droplets of diameters above 16 μm present. At XT, the peak of DNC is lower (see Fig. 3a), but the droplets spread over a wider size range, up to 25 μm. However, for the LWC$_{cum}$ (see Fig. 3b) the picture is completely different. At XT, the LWC$_{cum}$ is more than double as the one at AS. This aspect is due to the cubical relation of the diameter and the volume of spherical droplets. The 50% values of the LWC$_{cum}$ curves (Fig. 3b) are at 7 μm diameter for AS and at 15 μm for XT.

3.3. Time series of the fog events

The fog event of the 1st to 2nd March 2016 in AS (Fig. 4) began when visibility dropped below 1000 m) shortly before 20:00 (Fig. 4a). From 21:00 h to 07:00 h, visibility fell below 100 m with only a short break around 02:00 h. In the beginning of the fog event, all droplet sizes showed negative turbulent fluxes (see Fig. 4b). Soon after fog formation (around 19:00 h), some of the smallest droplet size classes changed their flux direction into positive fluxes. Other sizes, up to 10 μm in diameter, followed around 22:00 h. While the fluxes of droplets between 5 μm and 8 μm were mainly positive, droplet sizes between 8 μm and 10 μm changed their flux direction several times during the event. Fluxes of bigger droplets (⩾10 μm) were negative at all times. The orientation of size-resolved liquid water fluxes (see Fig. 4c) were, of course, in the same direction as the respective droplet number fluxes. However, because of the cubic relation between the liquid water flux and the number flux, the fluxes of middle-sized droplets (8 μm to 15 μm) dominated the LWF. Small droplet sizes exhibited only very low liquid water fluxes even with a large number flux because the volumes of these droplets are very small. The air temperature (see Fig. 4d) dropped down from 6 °C to 4 °C around sunset around 19:00 h. At 22:00 h, the air temperature rose again up to 7 °C and remained stable throughout the night. In the morning with the sunrise, the temperature started to rise continuously. Sensible heat flux (see Fig. 4e) decreased towards sunset, turned negative and remained so until 5:30 h when a small positive flux occurred that increased further with the dissipation of the fog around sunrise.

Fig. 5 shows the time series of a fog event at XT during the daytime of 9th March 2017. For the first time, the visibility dropped below 1000 m around 09:00 h (see Fig. 5a). From 11:30 h on, the visibility was extremely reduced (most of the time the visibility was ⩽50 m) for several hours until 20:00 h. This fog event (see Fig. 5b) had similar droplet number fluxes as the one at AS (see Fig. 4c). Around noon, fog occurred and the droplet number fluxes of all droplet sizes were negative, thus moving toward the surface. At 11:00 h, small droplets (3 μm) changed their flux direction to positive fluxes. Size classes up to a diameter of 10 μm followed at 12:00 h. The fluxes of small droplets continued to be positive until the end of the fog event at 20:00 h. Around 16:00 h, the fog was less dense and the droplet fluxes were small. As described for AS, the liquid water fluxes were in the same direction as the droplet number fluxes (see Fig. 5b&c). The air temperature (see Fig. 5d) was much higher compared to AS (see Fig. 4d). The temperature did rise in the morning from 13 °C to 15 °C and was somewhat reduced (to 13 °C) with the onset of fog at 11:30 h. The sensible heat flux (see Fig. 5e) rose with the sunrise at 8:00 h. The flux peaked at around 11:00 h and dropped with the formation of fog. The sensible heat flux stayed positive.

3.4. Critical diameters

The available aerosols grow due to heterogeneous nucleation, they are called CNN. Aerosols can only act as CNN if they are water-soluble (Stull, 2017), therefore the chemical composition of the aerosol

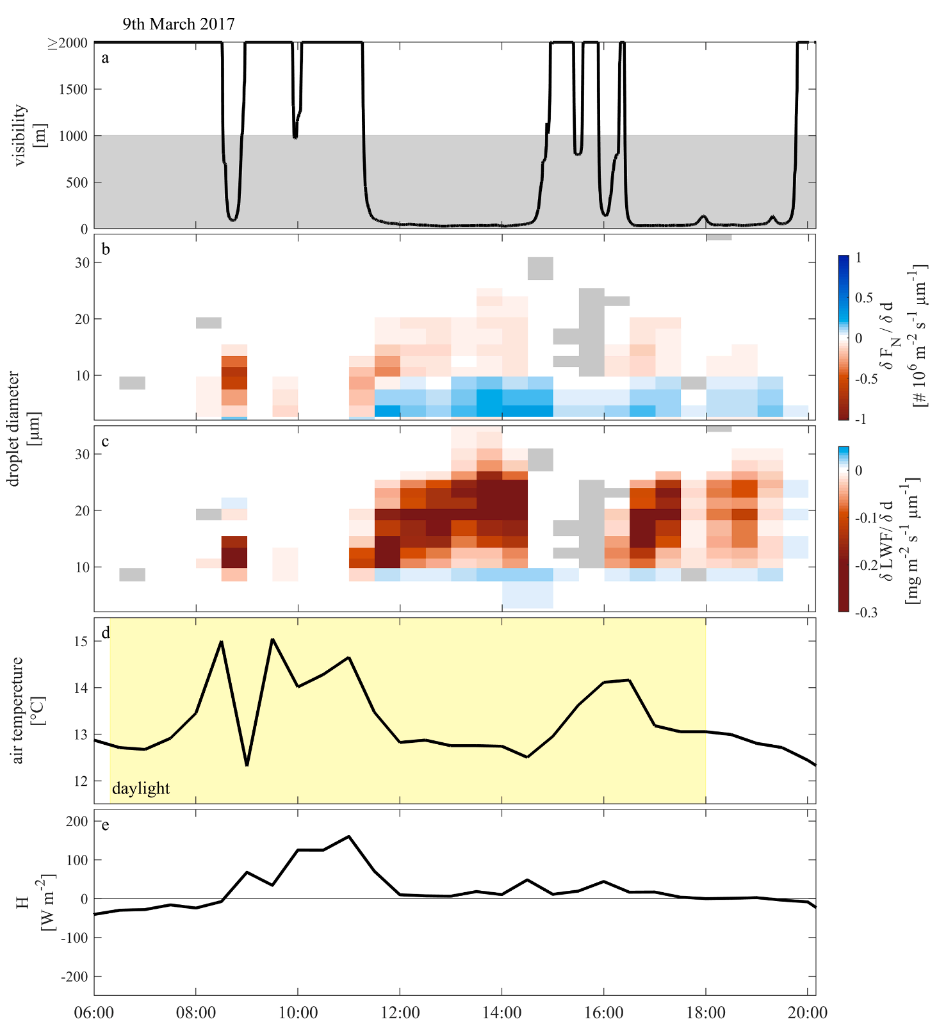

Fig. 5. Time series of the fog event on the 9th of March 2017 at XT showing the visibility (a), the normalized size-resolved droplet number flux (b), the normalized size-resolved LWF (c), the air temperature (d) and the sensible heat flux (e). The threshold of fog (visibility ⩽1000 m) is marked gray in panel a. Positive fluxes in panel b and c are shown in blue while negative fluxes are in red. Fluxes with bad quality flags (7, 8, 9) are denoted by gray pixels. White pixels are fluxes around zero, which also could be a result of low DNC.

particles is important. We estimated the critical diameters of the fog droplets for our two sites AS and XT as described in Section 2.4 above. The Kóhler curves for the fog events on the 1st/2nd March 2016 at AS and on the 9th March 2017 at XT are shown in Fig. 6. It is apparent that the critical diameters at the two sites are very different from each other. The lower IC at AS as compared to XT led to a generally lower critical diameter. The median droplet size diameter is similar at both sites, at around 7 µm. We conclude from this analysis of the critical diameters that at AS most of the droplets were activated, but at XT most of the droplets were non-activated. Note that the XT site is exposed to much higher levels of air pollution than the AS site (Simon et al., 2016; Nieberding et al., 2018). This leads to larger CCN, larger fog droplets, and to larger critical diameters at the XT site.

4. Discussion

The analysis of fog droplet fluxes at the two subtropical, forested mountainous sites revealed remarkable similarities. There was a net deposition flux of liquid water throughout the events, which is expected as a result of impaction of fog water droplets to the trees when transported to the respective surfaces through turbulence (El-Madany et al., 2016; Vermeulen et al., 1997; Holwerda et al., 2006). The size-resolved droplet number fluxes, however, showed positive fluxes for small droplets (<10 µm diameters) throughout rather long time periods of the events (several hours). Similar observations were made by El-Madany et al. (2016) at a different forest site (Chilan) in NE Taiwan. They argued that the respective droplets encounter warmer ambient air when moving downward, evaporate partially and thus decrease in size, and eventually are transported back upward again as smaller droplets through turbulent mixing. This process was associated with an positive sensible heat flux. The situation observed in the current study at XT is similar to that described by El-Madany et al. (2016), as the sensible heat fluxes during the occurrence of bidirectional fog droplet fluxes were positive. Note that the conditions at AS were different regarding one important aspect: The sensible heat fluxes during the time period of bidirectional fog droplet fluxes were negative. Therefore, the explanation offered by El-Madany et al. (2016), which also holds for XT, cannot explain the observed bidirectional fluxes at AS.

4.1. Sinks and sources of droplets

In the following, we disentangle the involved processes step by step in order to develop a general understanding of the conditions leading to the observed bidirectional fog droplet fluxes.

First we look at the processes at the canopy. The foggy air mass flows around leaves, twigs and branches, and the fog droplets follow the movement of the air. If the fog droplets cannot follow the streamlines of the turbulence elements, they impact at the canopy. In general, the canopy acts as a sink of all droplet sizes due to impaction. However, according to the Stokes' law smaller droplets can follow the streamlines better than bigger ones, while bigger droplets have a higher likelihood to impact (Seinfeld and Pandis, 2006). The Stokes' law generally describes the dependence of the frictional force of spherical bodies in a viscous fluid (Seinfeld and Pandis, 2006).

Other potential sinks and sources of droplets of given sizes are the growing and shrinking of droplets above the canopy yet inside the fog layer. No fog can be assumed to be a homogeneous isotherm or a perfectly adiabatically layered air mass. Instead, foggy layers contain air masses with higher RH and other air masses with lower RH (Pruppacher and Klett, 1996). Depending on the meteorological conditions that may have led to the formation of a specific fog, the vertical temperature gradient may be either positive or negative (Bruijnzeel et al., 2005). Therefore, individual fog droplets being transported upward or downward through turbulent motion may experience a transition from slightly lower RH to slightly higher RH or *vice versa*. This slight difference in RH around saturation or supersaturation will, generally speaking, lead to evaporation and condensation processes and, thus, to shrinking and growth of droplets during their vertical transport (Gerber, 1991; Gerber, 1980; Fritz et al., 2021; Li et al., 2019).

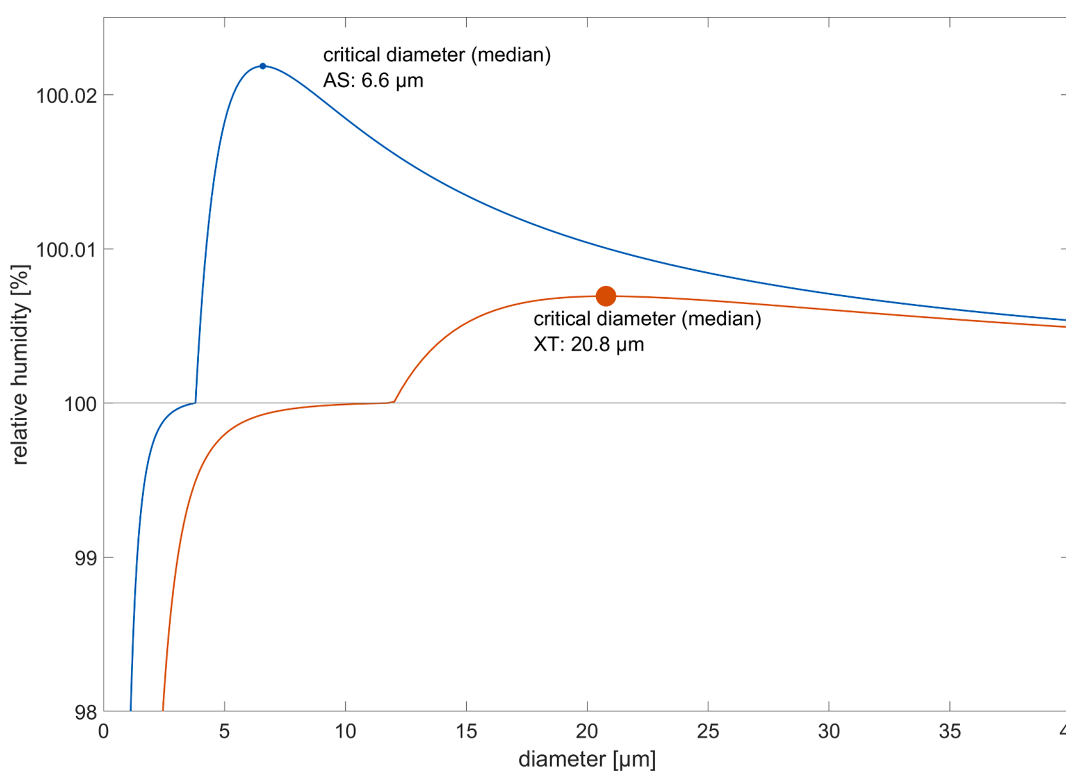

Fig. 6. Kóhler curves according to the particle mass for AS (blue) and XT (orange). Note the change of the scale of the y-axis above 100%. The median was calculated according to the chemical composition of the two example events (Table 2).

4.2. Heat fluxes

We do not have height-resolved temperature and relative humidity measurements at either site. However, the sensible heat flux clearly suggests the presence of a temperature difference with height, and this temperature gradient also affects the relative humidity. The flux direction of the sensible heat flux at AS is negative, while it is positive at XT (see Figs. 4e and 5e). Therefore, it is safe to state that the temperature at AS is cooler close to the surface than above. At XT we assume a higher temperature closer to the canopy than higher above.

4.3. Droplet activation and heat fluxes

Merging our knowledge about the droplet activation and the sensible heat flux, we propose mechanisms of droplet dynamics at XT and AS, respectively, as sketched in Fig. 7. The thermal layering of the fog layer at XT is opposite to what one would expect for radiation fog, but identical to that reported by El-Madany et al. (2016) for a similar mountain fog site in NE Taiwan: The upper air (above the instruments) is cooler than the lower air (see Section 4.2). The fog droplets consist mainly of non-activated droplets, such droplets evaporate partially during their turbulent transport downward. When moving upward, the droplets get into cooler air with higher RH and, thus, grow through condensation. The evaporation and condensation processes are faster than the transport of individual droplets, so smaller droplets (diameters <10 μm) move upward and larger droplets (>10 μm) move downward. Other experiments show an exchange time due to turbulence of around 90 s and a roughly estimated time for droplet growth from 0.25 μm to 17.33 μm (unpublished, Baumberger et al., 2021). This pattern explains the bidirectional flux pattern at XT (Fig. 5b&c). The lower part of the fog layer is considered a relative source of small droplets, whereas within the fog layer above the instruments, the droplets grow. Therefore, the upper air is a sink for small droplets.

The situation at AS is different in two ways. First, the thermal layering of foggy air is the opposite, in that cooler air with higher RH is below the instruments and warmer air is above. Second, the critical diameters of fog droplets are much smaller (Fig. 7, left panels). Through the combination of these conditions, the bidirectional flux pattern at AS is similar to that at XT: Large droplets are transported from above the instruments downward and reach more humid conditions. Note that the size ranges of droplets being transported upward was generally similar at AS and XT. Due the specific shape of the Kóhler curve at diameters larger than the critical diameters of the droplets, these droplets evaporate somewhat on their way down. Analogously, smaller droplets moving upward reach less humid air (yet still above 100% RH) but still grow in size (Fig. 7, left panels). In total, the number of small droplets transported upward was higher than the number of droplets transported downward. The fog layer above the instruments is a sink for small droplets and a source for big droplets due to condensation growth of the smaller droplets and reaching larger diameters.

5. Conclusion

Bidirectional droplet number fluxes were observed at two study sites and periods: In mainland China from January to March 2016 (AS: Ailaoshan National Natural Reserve in Yunnan Province, 24.54219 N, 101.02959 E, 2476 m asl) and in Taiwan in March 2017 (XT: Xitou, Experimental Forest of National Taiwan University in Nantou country, 23.66460 N, 120.79526 E, 1150 m asl). An approved setup of a eddy covariance system, including a droplet spectrometer (FM100 Fog Monitor), was used at both sites similar to El-Madany et al. (2016).

The normally expected flux direction for all droplet size classes is negative, toward the surface. However, we identified, as other studies have before, positive fluxes, upward into the atmosphere, for specific size classes. At both sites, droplets with sizes up to a 10 μm diameter showed positive fluxes at least temporarily during individual fog events.

To understand the processes inside the fog layer leading to these bidirectional fluxes, we merged our knowledge of droplet activation according to the Kóhler theory (Köhler, 1921) and the measured sensible heat fluxes. We verified two different cases of bidirectional droplet fluxes. At XT, the positive droplet number fluxes for smaller droplets (diameter up to 10 μm) occurred together with a positive sensible heat

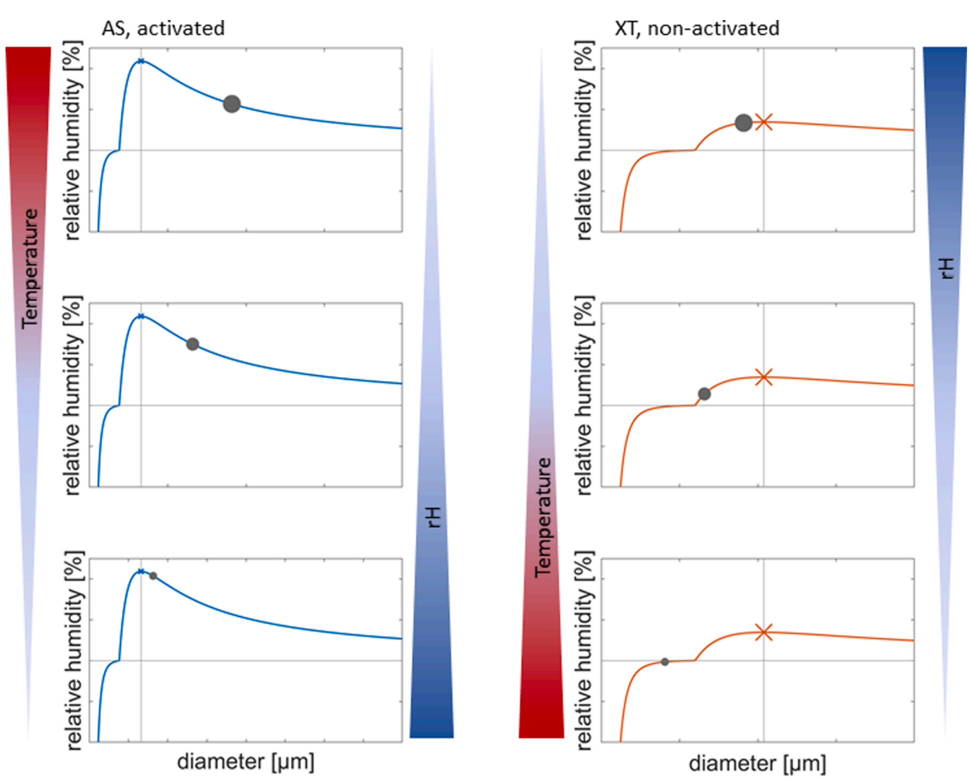

Fig. 7. Schematic of droplet growth and evaporation due to changes of the relative humidity with the turbulent up-and-down movement of fog droplets according to the respective Kóhler curve (Seinfeld and Pandis, 2006). The horizontal gray lines represent 100% RH; note the change of scale of y-axes at these points. The vertical gray lines represent the critical diameters of the respective study site. The right-hand orange curves represent the situation at XT, the left-hand side in blue stands for AS. The three graphs on top of each other (left and right, respectively) are symbolic for different heights above the canopy. The gray circles denote the sizes and positions of the droplets on the Kóhler curves. The temperature and relative humidity gradients are shown. The gradients, are oriented opposite to each other at the two study sites.

flux in combination with large critical diameters, while at AS, the same fluxes occurred with negative sensible heat fluxes in combination with small critical diameters.

In the end, bidirectional droplet number fluxes are caused by the (I) boundary layer conditions, particularly regarding the sensible heat flux, from which we conclude a temperature and humidity gradient with height, and (II) the size and chemical composition of available CCN for the droplets to form via condensation.

Our study supports the general understanding that liquid water is deposited to ecosystems' surfaces and, thus, impacts their hydrological budgets. The involved process are, however, much more complex. The interaction between energy fluxes and microphysics of droplets under various boundary conditions suggests a far more complex picture, in which droplets of various sizes exhibit varying flux directions. As such, the involved processes should be studied in more detail. Further investigations are needed to understand all processes inside of the fog layer. We suggest that further studies measure temperature and humidity precisely in a height profile, measure droplet sizes over a wider size range, and measure both dry and wet particles (size and chemical composition) before the onset of fog events as well as during long-term investigations. Such studies should also include turbulent fluxes and the chemical compositions of non-activated droplets with sizes under 2 μm in diameter.

6. Authors contributions

Bettina Breuer: Methodology, Software, Validation, Formal analysis, Investigation, Data Curation, Writing - Original Draft, Visualization. **Otto Klemm**: Conceptualization, Methodology, Resources, Writing - Review & Editing, Supervision, Project administration, Funding acquisition. **Yen-Jen Lai**: Investigation, Resources, Funding acquisition. **Po–Hsiung Lin**: Investigation, Resources, Funding acquisition. **Heta Meyer**: Software, Formal analysis, Investigation, Data Curation. **Felix Nieberding**: Investigation. **Qing-Hai Song**: Investigation, Resources, Funding acquisition.

Declaration of Competing Interest

The authors declare that they have no known competing financial interests or personal relationships that could have appeared to influence the work reported in this paper.

Acknowledgments

This work was financially supported by the German Academic Exchange Service (DAAD) and the Ministry of Science and Technology of Taiwan (MOST) within their PPP program "Studies on Fog and Cloud Chemistry with Optimized Temporal Resolution". This project was supported by the National Natural Science Foundation of China (41671209). We thank Celeste Brennecka for language editing of the manuscript. Two anonymous reviewers helped with their useful comments to improve our manuscript.

References

Beiderwieden, E., Schmidt, A., Hsia, Y.J., Chang, S.C., Wrzesinsky, T., Klemm, O., 2007. Nutrient input through occult and wet deposition into a subtropical montane cloud forest. Water Air Soil Pollut. 186, 273–288. https://doi.org/10.1007/s11270-007-9483-0.

Beiderwieden, E., Wolff, V., Hsia, Y.J., Klemm, O., 2008. It goes both ways: Measurements of simultaneous evapotranspiration and fog droplet deposition at a montane cloud forest. Hydrol. Process. 22, 4181–4189. https://doi.org/10.1002/Hyp.7017.

Best, A.C., 1951. Drop-Size Distribution in Cloud and Fog. Quart. J. R. Meteorol. Soc. 77, 418–426. https://doi.org/10.1002/qj.49707733307.

Beswick, K.M., Hargreaves, K.J., Gallagher, M.W., Choularton, T.W., Fowler, D., 1991. Size-resolved measurements of cloud droplet deposition velocity to a forest canopy using an eddy-correlation technique. Q.J.R. Meteorol. Soc. 117, 623–645. https://doi.org/10.1002/qj.49711749910.

Brock, F.V., 1986. A nonlinear filter to remove impulse noise from meteorological data. J. Atmos. Ocean. Technol. 3, 51–58. https://doi.org/10.1175/1520-0426(1986)003<0051:ANFTRI>2.0.CO;2.

Bruijnzeel, L.A., Eugster, W., Burkard, R., 2005. Fog as a Hydrological Input, in: Anderson, M.G. (Ed.), Encyclopedia of Hydrological Sciences. J. Wiley, Chichester, West Sussex, England, Hoboken, NJ. volume 4, pp. 559–582.

Burkard, R., Butzberger, P., Eugster, W., 2003. Vertical fogwater flux measurements above an elevated forest canopy at the Lageren research site, Switzerland. Atmos. Environ. 37, 2979–2990. https://doi.org/10.1016/S1352-2310(03)00254-1.

Chang, S.C., Yeh, C.F., Wu, M.J., Hsia, Y.J., Wu, J.T., 2006. Quantifying fog water deposition by in situ exposure experiments in a mountainous coniferous forest in Taiwan. For. Ecol. Manage. 224, 11–18. https://doi.org/10.1016/j.foreco.2005.12.004.

Degefie, D., El-Madany, T.S., Held, M., Hejkal, J., Hammer, E., Dupont, J.C., Haeffelin, M., Fleischer, E., Klemm, O., 2015b. Fog chemical composition and its feedback to fog water fluxes, water vapor fluxes, and microphysical evolution of two events near Paris. Atmos. Res. 164–165, 328–338. https://doi.org/10.1016/j.atmosres.2015.05.002.

Degefie, D., El-Madany, T.S., Hejkal, J., Held, M., Dupont, J.C., Haeffelin, M., Klemm, O., 2015a. Microphysics and energy and water fluxes of various fog types at SIRTA, France. Atmos. Res. 151, 162–175. https://doi.org/10.1016/j.atmosres.2014.03.016.

El-Madany, T.S., Walk, J.B., Deventer, M.J., Degefie, D.T., Chang, S.C., Juang, J.Y., Griessbaum, F., Klemm, O., 2016. Canopy-atmosphere interactions under foggy condition—Size-resolved fog droplet fluxes and their implications. J. Geophys. Res.: Biogeosci. 121, 796–808. https://doi.org/10.1002/2015JG003221.

Eugster, W., Burkard, R., Holwerda, F., Scatena, F.N., Bruijnzeel, L.A.S., 2006. Characteristics of fog and fogwater fluxes in a Puerto Rican elfin cloud forest. Agric. For. Meteorol. 139, 288–306. https://doi.org/10.1016/j.agrformet.2006.07.008.

Foken, T., Wichura, B., 1996. Tools for quality assessment of surface-based flux measurements. Agric. For. Meteorol. 78, 83–105. https://doi.org/10.1016/S1352-2310(96)00056-8.

Foken, T., Göckede, M., Mauder, M., Mahrt, L., Amiro, B., Munger, J., 2004. Post-field data quality control. In: Lee, X., Massman, W., Law, B. (Eds.), Handbook of Micrometeorology: A Guide for Surface Flux Measurement and Analysis. Kluwer Academic Publishers, Dordrecht, pp. 181–208.

Fritz, J., Meyer, H., Tseng, W., Lin, N.H., Klemm, O., 2021. Covariation of droplet size distribution and air humidity in fog: A methodological approach. J. Hydrol. 594, 125934 https://doi.org/10.1016/j.jhydrol.2020.125934.

Gallagher, M.W., Choularton, T.W., Morse, A.P., Fowler, D., 1988. Measurements of the size dependence of cloud droplet deposition at a hill site. Quart. J. R. Meteorol. Soc. 114, 1291–1303. https://doi.org/10.1002/qj.49711448307.

Gallagher, M.W., Beswick, K., Choularton, T.W., Coe, H., Fowler, D., Hargreaves, K., 1992. Measurements and modelling of cloudwater deposition to moorland and forests. Environ. Pollut. 75, 97–107. https://doi.org/10.1016/0269-7491(92)90062-F.

Gerber, H.E., 1980. A saturation hygrometer for the measurement of relative-humidity between 95-percent and 105-percent. J. Appl. Meteorol. 19, 1196–1208. https://doi.org/10.1175/1520-0450(1980)019<1196:ASHFTM>2.0.CO;2.

Gerber, H., 1991. Supersaturation and droplet spectral evolution in fog. J. Atmos. Sci. 48, 2569–2588. https://doi.org/10.1175/1520-0469(1991)048<2569:SADSEI>2.0.CO;2.

Gonser, S., Klemm, O., Griessbaum, F., Chang, S.C., Chu, H.S., Hsia, Y.J., 2011. The relation between humidity and liquid water content in fog: an experimental approach. Pure Appl. Geophys. 169, 821–833. https://doi.org/10.1007/s00024-011-0270-x.

Gultepe, I., Isaac, G., 2004. Aircraft observations of cloud droplet number concentration: Implications for climate studies. Quart. J. R. Meteorol. Soc. 130, 2377–2390. https://doi.org/10.1256/qj.03.120.

Gultepe, I., Tardif, R., Michaelides, S.C., Cermak, J., Bott, A., Bendix, J., Muller, M.D., Pagowski, M., Hansen, B., Ellrod, G., Jacobs, W., Toth, G., Cober, S.G., 2007. Fog research: A review of past achievements and future perspectives. Pure Appl. Geophys. 164, 1121–1159. https://doi.org/10.1007/s00024-007-0211-x.

Hewson, E.W., 1943. The reflection, absorption, and transmission of solar radiation by fog and cloud. Quart. J. R. Meteorol. Soc. 69, 47–62. https://doi.org/10.1002/qj.49706929808.

Hiatt, C., Fernandez, D., Potter, C., 2012. Measurements of fog water deposition on the california central coast. Atmos. Clim. Sci. 02, 525–531. https://doi.org/10.4236/acs.2012.24047.

Holwerda, F., Burkard, R., Eugster, W., Scatena, F.N., Meesters, A.G.C.A., Bruijnzeel, L. A., 2006. Estimating fog deposition at a Puerto Rican elfin cloud forest site: Comparison of the water budget and eddy covariance methods. Hydrol. Process. 20, 2669–2692. https://doi.org/10.1002/hyp.6065.

Horst, T.W., 1997. A simple formula for attenuation of eddy fluxes measured with first-order-response scalar sensors. Bound.-Lay. Meteorol. 82, 219–233. https://doi.org/10.1023/A:1000229130034.

Klemm, O., Wrzesinsky, T., 2007. Fog deposition fluxes of water and ions to a mountainous site in Central Europe. Tellus B 59, 705–714. https://doi.org/10.1111/j.1600-0889.2007.00287.x.

Köhler, H., 1921. Zur Kondensation des Wasserdampfes in der Atmosphäre. Geof. Publ. 2, 3–15.

Kowalski, A.S., Vong, R.J., 1999. Near-surface fluxes of cloud water evolve vertically. Q.J.R. Meteorol. Soc. 125, 2663–2684. https://doi.org/10.1002/qj.49712555916.

Li, X.Y., Svensson, G., Brandenburg, A., Haugen, N.E.L., 2019. Cloud-droplet growth due to supersaturation fluctuations in stratiform clouds. Atmos. Chem. Phys. 19, 639–648. https://doi.org/10.5194/acp-19-639-2019 arXiv:1806.10529.

Lovett, G.M., 1984. Rates and mechanisms of cloud water deposition to a subalpine balsam fir forest. Atmos. Environ. 18, 361–371. https://doi.org/10.1016/0004-6981(84)90110-0.

Mammarella, I., Peltola, O., Nordbo, A., Järvi, L., Rannik, Ü., 2016. EddyUH: An advanced software package for eddy covariance flux calculation for a wide range of instrumentation and ecosystems. Atmos. Measur. Tech. Discuss. 1, 1–33. https://doi.org/10.5194/amt-2015-323.

Mie, G., 1908. Beiträge zur Optik trüber Medien, speziell kolloidaler Metallösungen. Ann. Phys. 4, 377–445. https://doi.org/10.1002/andp.19083300302.

Mildenberger, K., Beiderwieden, E., Hsia, Y.J., Klemm, O., 2009. CO2 and water vapor fluxes above a subtropical mountain cloud forest-The effect of light conditions and fog. Agric. For. Meteorol. 149, 1730–1736. https://doi.org/10.1016/j.agrformet.2009.06.004.

Moncrieff, J.B., Massheder, J.M., deBruin, H., Elbers, J., Friborg, T., Heusinkveld, B., Kabat, P., Scott, S., Soegaard, H., Verhoef, A., 1997. A system to measure surface fluxes of momentum, sensible heat, water vapour and carbon dioxide. J. Hydrol. 189, 589–611. https://doi.org/10.1016/S0022-1694(96)03194-0.

Nieberding, F., 2017. Fogwater chemical composition at ailaoshan mountain, Yunnan Province, SW China. Master thesis. Westfälische Wilhelms-Universität Münster, Münster.

Nieberding, F., Breuer, B., Braeckevelt, E., Klemm, O., Song, Q., Zhang, Y., 2018. Fog water chemical composition on ailaoshan mountain, Yunnan Province, SW China. Aerosol. Air Quality Res. 18, 37–48. https://doi.org/10.4209/aaqr.2017.01.0060.

Paw U.K.T., Baldocchi, D.D., Meyers, T.P., Wilson, K.B., 2000. Corrections of eddy covariance measurements incorporating both advective effects and density fluxes. Bound.-Layer Meteorol. 97, 487–511. 10.1023/A:1002786702909.

Petterssen, S., 1939. Some aspects of formation and dissipation of fog. Geof. Publ. XII, 5–22.

Pruppacher, H.R., Klett, J.D., 1996. Microphysics of clouds and precipitation. Atmospheric and Oceanographic Sciences Library v. 18. 2 ed., Kluwer Academic Publishers, Dordrecht; Boston.

Rannik, U., Vesala, T., 1999. Autoregressive filtering versus linear detrending in estimation of fluxes by the eddy covariance method. Bound.-Layer Meteorol. 91, 259–280. https://doi.org/10.1023/A:1001840416858.

Savitzky, A., Golay, M.J.E., 1964. Smoothing + differentiation of data by simplified least squares procedures. Anal. Chem. 36, 1627–1639. https://doi.org/10.1021/ac60214a047.

Schaefer, D.A., Feng, W., Zou, X., 2009. Plant carbon inputs and environmental factors strongly affect soil respiration in a subtropical forest of southwestern China. Soil Biol. Biochem. 41, 1000–1007. https://doi.org/10.1016/j.soilbio.2008.11.015.

Seinfeld, J.H., Pandis, S.N., 2006. Atmospheric chemistry and physics: from air pollution to climate change, 2nd ed. J. Wiley, Hoboken, N.J.

Shi, J.P., Zhu, H., 2009. Tree species composition and diversity of tropical mountain cloud forest in the Yunnan, southwestern China. Ecol. Res. 24, 83–92. https://doi.org/10.1007/s11284-008-0484-2.

Simon, S., Klemm, O., El-Madany, T., Walk, J., Amelung, K., Lin, P.H., Chang, S.C., Lin, N.H., Engling, G., Hsu, S.C., Wey, T.H., Wang, Y.N., Yu-Chi, Lee, 2016. Chemical composition of fog water at four sites in Taiwan. Aerosol Air Quality Res. 16, 618–631. https://doi.org/10.4209/aaqr.2015.03.0154.

Song, Q.H., Braeckevelt, E., Zhang, Y.P., Sha, L.Q., Zhou, W.J., Liu, Y.T., Wu, C.S., Lu, Z. Y., Klemm, O., 2017. Evapotranspiration from a primary subtropical evergreen forest in Southwest China. Ecohydrology 10. https://doi.org/10.1002/eco.1826 n/a–n/a.

Sperling, F.N., Washington, R., Whittaker, R.J., 2004. Future climate change of the subtropical north atlantic: implications for the cloud forests of tenerife. Climatic Change 65, 103–123. https://doi.org/10.1023/B:CLIM.0000037488.33377.bf.

Spiegel, J.K., Zieger, P., Bukowiecki, N., Hammer, E., Weingartner, E., Eugster, W., 2012. Evaluating the capabilities and uncertainties of droplet measurements for the fog droplet spectrometer (FM-100). Atmos. Measur. Tech. 5, 2237–2260. https://doi.org/10.5194/amt-5-2237-2012.

Stull, R., 2017. Practical meteorology: an algebra-based survey of atmospheric science. Univ. of British Columbia, Vancouver. OCLC: 41719512.

Tan, Z.H., Zhang, Y.P., Schaefer, D., Yu, G.R., Liang, N.S., Song, Q.H., 2011. An old-growth subtropical Asian evergreen forest as a large carbon sink. Atmos. Environ. 45, 1548–1554. https://doi.org/10.1016/j.atmosenv.2010.12.041.

Thalmann, E., Burkard, R., Wrzesinsky, T., Eugster, W., Klemm, O., 2002. Ion fluxes from fog and rain to an agricultural and a forest ecosystem in Europe. Atmos. Res. 64, 147–158. https://doi.org/10.1016/S0169-8095(02)00087-X.

Vermeulen, A., Wyers, G., Römer, F., Van Leeuwen, N., Draaijers, G., Erisman, J., 1997. Fog deposition on a coniferous forest in The Netherlands. Atmos. Environ. 31, 375–386. https://doi.org/10.1016/S1352-2310(96)00056-8.

Vickers, D., Mahrt, L., 1997. Quality control and flux sampling problems for tower and aircraft data. J. Atmos. Ocean. Technol. 14, 512–526. https://doi.org/10.1175/1520-0426(1997)014<0512:QCAFSP>2.0.CO;2.

Vong, R.J., Kowalski, A.S., 1995. Eddy correlation measurements of size-dependent cloud droplet turbulent fluxes to complex terrain. Tellus Series B 47, 331–352. https://doi.org/10.1034/j.1600-0889.47.issue3.5.x.

Wilczak, J.M., Oncley, S.P., Stage, S.A., 2001. Sonic anemometer tilt correction algorithms. Bound.-Layer Meteorol. 99, 127–150. https://doi.org/10.1023/A:1018966204465.

Willett, H.C., 1928. Fog and haze, their causes, distribution, and forecasting. Mon. Weather Rev. 56, 435–468. https://doi.org/10.1175/1520-0493(1928)56<435:FAHTCD>2.0.CO;2.

WMO, 2006. Initial guidance to obtain representative meteorological observations at urban sites. Instrum. Observ. Meth. 81. WMO/TD-No. 1250.

Wrzesinsky, T., 2003. Direkte Messung und Bewertung des nebelgebundenen Eintrags von Wasser und Spurenstoffen in ein montanes Waldökosystem. Inauguraldissertation. Universität Bayreuth. Bayreuth.

Yamaguchi, T., Katata, G., Noguchi, I., Sakai, S., Watanabe, Y., Uematsu, M., Furutani, H., 2015. Long-term observation of fog chemistry and estimation of fog water and nitrogen input via fog water deposition at a mountainous site in Hokkaido, Japan. Atmos. Res. 151, 82–92. https://doi.org/10.1016/j.atmosres.2014.01.023.

Zhou, G., Peng, C., Li, Y., Liu, S., Zhang, Q., Tang, X., Liu, J., Yan, J., Zhang, D., Chu, G., 2013. A climate change-induced threat to the ecological resilience of a subtropical monsoon evergreen broad-leaved forest in Southern China. Glob. Change Biol. 19, 1197–1210. https://doi.org/10.1111/gcb.12128.